

Atmospheric characterization of hot Jupiters using hierarchical models of *Spitzer* observations

Dylan Keating,^{1*} Nicolas B. Cowan,^{1,2}

¹*Department of Physics, McGill University, Montréal, QC H3A 2T8, Canada*

²*Department of Earth & Planetary Sciences, McGill University, Montréal, QC H3A 2T8, Canada*

Submitted 2021 February 25

ABSTRACT

The field of exoplanet atmospheric characterization is trending towards comparative studies involving many planets, and using hierarchical modelling is a natural next step. Here we demonstrate two use cases. We first use hierarchical modelling to quantify variability in repeated observations, by reanalyzing a suite of ten *Spitzer* secondary eclipse observations of the hot Jupiter XO-3b. We compare three models: one where we fit ten separate eclipse depths, one where we use a single eclipse depth for all ten observations, and a hierarchical model. By comparing the Widely Applicable Information Criterion (WAIC) of each model, we show that the hierarchical model is preferred over the others. The hierarchical model yields less scatter across the suite of eclipse depths, and higher precision on the individual eclipse depths, than does fitting the observations separately. We do not detect appreciable variability in the secondary eclipses of XO-3b, in line with other analyses. Finally, we fit the suite of published dayside brightness measurements from Garhart et al. (2020) using a hierarchical model. The hierarchical model gives tighter constraints on the individual brightness temperatures and is a better predictive model, according to the WAIC. Notably, we do not detect the increasing trend in brightness temperature ratios versus stellar irradiation reported by Garhart et al. (2020) and Baxter et al. (2020). Although we tested hierarchical modelling on *Spitzer* eclipse data of hot Jupiters, it is applicable to observations of smaller planets like hot neptunes and super earths, as well as for photometric and spectroscopic transit or phase curve observations.

Key words: planets and satellites: individual (XO-3b) – techniques: photometric

1 INTRODUCTION

Although the *Spitzer Space Telescope* wasn't designed for exoplanet science, it was a workhorse for the field. In particular, observations of exoplanet transits, secondary eclipses, and phase curves with *Spitzer's* Infrared Array Camera have been used to characterize the atmospheres of over a hundred transiting planets.

Substantial progress has been made towards a statistical understanding of exoplanetary atmospheres (Cowan & Agol 2011; Sing et al. 2016; Schwartz & Cowan 2015; Schwartz et al. 2017; Parmentier & Crossfield 2018; Zhang et al. 2018; Keating et al. 2019, 2020; Baxter et al. 2020; Bell et al. 2020). Many of the planets in these studies had been analyzed using disparate reduction and analysis pipelines, but recently the field has been moving towards analyzing suites of observations from multiple planets using a single pipeline. Garhart et al. (2020) independently reduced and analyzed 78 eclipse depths from 36 planets and found that hotter planets had higher brightness temperatures at 4.5 μm than at 3.6 μm . Bell et al. (2020) reanalyzed every available *Spitzer* 4.5 μm hot Jupiter phase curve using an open-source reduction and analysis pipeline, confirming several previously reported trends.

In this work we outline a complementary way to further the statistical understanding of exoplanet atmospheres: fitting measurements

from multiple planets simultaneously using hierarchical models to robustly infer trends.

1.1 *Spitzer* Systematics

Exoplanet observations taken with *Spitzer's* Infrared Array Camera (IRAC; Fazio et al. (2004)) are dominated by systematics noise. The systematics are driven by intrapixel sensitivity variations on the detector and by now are well characterized (Ingalls et al. 2016). The detector systematics are typically fitted simultaneously with the astrophysical signal of interest. Each transit, secondary eclipse, and phase curve yields information about the IRAC detector sensitivity, but typically this information is not shared between observations.

Since the *Spitzer* systematics are a function of the centroid location on the pixel, efforts have been made to determine the detector sensitivity independently using observations of quiet stars (Ingalls et al. 2012; Krick et al. 2020; May & Stevenson 2020). The flux of a calibration star should be constant as a function of time, so any deviation must be due to the centroid moving across the detector as the telescope pointing drifts. A crucial assumption for this approach is that the *Spitzer* systematics do not vary with time, and that they are not dependent on the brightness of the star. Ingalls et al. (2012) and May & Stevenson (2020) approached the problem by explicitly calculating the detector sensitivity, while Krick et al. (2020) used a

* E-mail: dylan.keating@mail.mcgill.ca

machine learning technique called random forests to look for patterns in the systematics.

Other approaches do not assume anything explicit about the detector sensitivity. Independent component analysis (Waldmann 2012; Morello et al. 2014, 2016) separates the signal into additive subcomponents using blind source separation, with the idea being that one of these signals is the astrophysical signal. In another approach, Morvan et al. (2020) used the baseline signal before and after a transit to learn and predict the in transit detector systematics using a machine learning technique known as Long short-term memory networks.

In this work, we opted to model and fit the detector systematics to allow for any correlations between the systematics and astrophysical signals.

1.2 Hierarchical Models

Hierarchical models (Gelman et al. 2014) are routinely used in other fields because they offer a natural way to infer higher level trends that exist in a dataset, and can increase measurement precision. They are gaining traction in exoplanet studies: for example, to study the mass-radius (Teske et al. 2020) and mass-radius-period (Neil & Rogers 2020) relations, and radius inflation of hot Jupiters (Sarkis et al. 2021; Thorngren et al. 2021). Hierarchical models have not yet been applied to atmospheric characterization of exoplanets.

There is one major difference between a typical Bayesian model and a hierarchical one. In a hierarchical model one assumes that some of the model parameters of interest are drawn from a higher level, unobserved distribution. The higher level parameters describing this distribution, otherwise known as hyperparameters, are fitted simultaneously with the parameters of interest. As we explain below, this naturally represents how our intuition pools information across observations. It also helps to tame models by compromising between overfitting and underfitting.

Hierarchical models can and should be used whenever a higher level structure can be assumed in a data set, such as when one quantity is measured multiple times. A natural example is the archetypical suite of ten XO-3b *Spitzer* IRAC Channel 2 (4.5 μm) eclipses (Wong et al. 2014). Below we explain the model and present results. Afterwards, we show how we extend the model to fit multiple eclipses from different planets simultaneously and present results from fitting the eclipse data from Garhart et al. (2020) with a hierarchical model.

2 HIERARCHICAL MODEL OF XO-3B ECLIPSES

In the *Spitzer* data challenge, several groups analyzed ten secondary eclipses of XO-3b in order to test repeatability and accuracy of various decorrelation techniques (Ingalls et al. 2016). The reduced archival data from the data challenge are publicly available, so we downloaded them rather than reducing them ourselves.

For XO-3b and other planets with repeated secondary eclipse observations, the eclipses have usually been fitted separately from one another, with a separate eclipse depth parameter for each observation (Ingalls et al. 2016; Kilpatrick et al. 2020). In other cases, a single eclipse depth parameter has been used to simultaneously fit multiple secondary eclipse measurements (Wong et al. 2014). This is also what is typically done for phase curves that are bracketed by two eclipses (Cowan et al. 2012; Bell et al. 2020).

However, neither approach quite matches what our intuition tells us. Because we are measuring the same thing each time, fitting the eclipse observations separately amounts to overfitting the individual observations, and fitting a single eclipse parameter amounts to

underfitting all of the observations. If we observe one secondary eclipse, we would expect that the next one we observe would have a similar— but not identical— depth, due to measurement uncertainty, if not astrophysical variability. The second eclipse we observe would also change our beliefs about the first one. Each measurement of the planet’s eclipse depth can be thought of as a draw from a distribution, with some variance. With enough measurements, the shape of this distribution can be inferred. A hierarchical model naturally takes all of this into account by fitting for the parameters that describe the higher level distribution simultaneously with the astrophysical signal of each observation.

Bayesian analysis requires us to specify priors on the parameters we are trying to infer. We can write down our prior on the i th eclipse depth as

$$ED_i \sim \mathcal{N}(\mu, \sigma), \quad (1)$$

where we have used shorthand to say that the eclipse depth is drawn from a normal distribution centered on μ with a standard deviation of σ ; μ and σ are hyperparameters. In a non-hierarchical model, we would specify values μ and σ to represent our prior expectations of what ED_i could be. After fitting, we would get a separate posterior distribution for each eclipse depth.

In a hierarchical model, we instead make μ and σ parameters and fit them simultaneously with the ten eclipse depths. We represent our beliefs about hyperparameters μ and σ with hyperpriors. This allows each eclipse observation to inform the others, by pulling the eclipse depths closer to the mode of the distribution of μ . This is known as Bayesian shrinkage. After fitting, we get a posterior distribution for each eclipse depth, as well as for μ and σ .

In the limit that σ goes to infinity, the hierarchical model is equivalent to the model with completely separate eclipse depths. Likewise when σ goes to zero, it is equivalent to the single eclipse depth model. A hierarchical model empirically fits for the amount of pooling based on what is most consistent with the observations.

2.1 Priors

Priors are necessary in a model to encode prior knowledge, as well as to properly sample a model. In all cases, we use weakly informative priors rather than flat, “uninformative” priors. Half-normal priors or wide normal priors are unlikely to introduce much bias into the parameter estimates and can make sampling more efficient. Flat priors are discouraged in practice because we usually have at least some vague knowledge of the range of values a parameter can take (Gelman et al. 2017).

For instance, consider a flat prior on the eclipse depth. This is equivalent to saying that all values of eclipse depth are equally likely, even extremely large, unphysical values. Instead, we chose to place a normal prior with a large standard deviation so that we kept the predicted values within the right order of magnitude.

2.2 Astrophysical Model

The astrophysical model for each observation was a secondary eclipse. We used STARRY (Luger et al. 2019) to compute the shape of each eclipse, with the depth and time of eclipse left as free parameters. We fixed the radius of the planet and host star, the orbital period, ratio of semi-major axis to stellar radius, orbital inclination, longitude of periastron and eccentricity to the literature values.

To get a rough upper limit on the eclipse depth, we used the parameterization of Cowan & Agol (2011) to calculate the maximum

dayside temperature, in the limit of a Bond albedo of zero and no heat recirculation:

$$T_{d,\max} = T_{\text{eff}} \sqrt{\frac{R_{\star}}{a}} \left(\frac{2}{3}\right)^{1/4}. \quad (2)$$

Here T_{eff} is the stellar effective temperature, and a/R_{\star} is the ratio of semimajor axis to stellar radius. We note that this equation assumes a circular orbit, while XO-3b is on an eccentric orbit ($e = 0.28$; Bonomo et al. (2017)). Nonetheless, it allows us to get an order of magnitude estimate of the eclipse depth.

The above temperature can be converted to an eclipse depth using

$$ED = \frac{B(\lambda, T_d)}{B(\lambda, T_{\star, 4.5\mu\text{m}})} \left(\frac{R_p}{R_{\star}}\right)^2 \quad (3)$$

where B is the Planck function, and $T_{\star, 4.5\mu\text{m}}$ is the brightness temperature of the star at $4.5 \mu\text{m}$, which we calculated by integrating PHOENIX models (Allard et al. 2011) over the *Spitzer* bandpass (Baxter et al. 2020).

For the non-hierarchical model, we placed a wide prior on the eclipse depth to prevent biasing the value: $ED \sim \mathcal{N}(ED_{\max}/2, ED_{\max}/2)$. For the time of eclipse, we let $\tau \sim \mathcal{N}(\Delta t/2, \Delta t/2)$ where Δt is the duration of the observation, and time is measured from the start of the observation. We experimented with various priors and found that our resulting fits were consistent and not strongly dependent on the choice of priors.

For the hierarchical model, we used a wide Normal prior for the hierarchical mean: $\mu \sim \mathcal{N}(ED_{\max}/2, ED_{\max}/2)$. For the hierarchical standard deviation we used a weakly informative Half-Normal prior: $\sigma \sim \text{Half-}\mathcal{N}(300\text{ppm})$. We then let the individual eclipse depths be drawn from the following higher level distribution: $ED_i \sim \mathcal{N}(\mu, \sigma)$

2.3 Detector Systematics: Gaussian Processes

The IRAC detector sensitivity in Channels 1 and 2 depends on the target centroid position on the detector. To parameterize this behaviour, we used a Gaussian process. The advantage of using a Gaussian process is that it doesn't require calculating the detector sensitivity explicitly, in contrast with polynomial models (Cowan et al. 2012) or BLISS (Stevenson et al. 2012).

When using Gaussian processes, we make the usual assumption that the data are normally distributed, but allow for covariance between data points. The likelihood function can be written

$$p(\text{data}|\gamma) \sim \mathcal{N}(\mu_{\text{GP}}, \Sigma), \quad (4)$$

where γ represents the model parameters and independent variables, and μ_{GP} is the mean function around which the data are distributed. The covariance function, Σ , is an $n \times n$ matrix where n is the number of data. The entries along the diagonal of Σ are the measurement uncertainties on each datum, and the off-diagonal entries are the covariance between data. When the off-diagonal elements are equal to zero, the likelihood function reduces to the usual assumption of independent Gaussian uncertainties.

Although it is computationally intractable to fit each off-diagonal entry of the covariance matrix, they can be parameterized using a kernel function with a handful of parameters. We used the squared exponential kernel employed by Evans et al. (2015)

$$\Sigma_{ij} = \alpha \exp \left[-\left(\frac{x_i - x_j}{l_x}\right)^2 - \left(\frac{y_i - y_j}{l_y}\right)^2 \right], \quad (5)$$

where x and y represent the centroid locations on the IRAC detector, in pixel coordinates. The terms l_x and l_y are the covariance lengthscales, and α is the Gaussian process amplitude. The squared exponential kernel has the intuitive property that locations on the detector pixel that are close together should have similar sensitivity. If the length scales are fixed by the user rather than fitted for, this boils down to the Gaussian kernel regression of Knutson et al. (2012) and Lewis et al. (2013)

With no loss of generality, we can let the mean function be zero, and instead fit the residuals between the astrophysical model and observations which gives

$$p(\text{residuals}|\gamma) \sim \mathcal{N}(0, \Sigma). \quad (6)$$

We placed weakly informative inverse gamma priors on the lengthscales. We chose the parameters such that 99% of the prior probability was between lengthscales 0 and 1, measured in pixels. This gives $p(l_x), p(l_y) \sim \text{InverseGamma}(\alpha=11, \beta=5)$.

For the amplitude α , we used a weakly informative half normal prior: $\alpha \sim \text{Half-}\mathcal{N}(0, \Delta F/3)$, where $\Delta F/3$ is the range of observed flux values. By using a half normal prior, we weakly constrain the scale of the Gaussian process amplitude without introducing bias. We placed the same prior on the white noise uncertainty, σ_{phot} .

2.4 The posterior

For each eclipse, we fit the eclipse depth ED , time of eclipse τ , photometric uncertainty σ_{phot} , Gaussian process lengthscales l_x and l_y , and Gaussian process amplitude α . The planet-to-star flux ratio as a function of time t is given by F . The x and y centroid locations are included as covariates. We also fit for the hierarchical eclipse depth mean μ , and standard deviation σ .

The likelihood function for one eclipse is given by

$$p(F|t, x, y, \sigma_{\text{phot}}, ED, \mu, \sigma, \tau, l_x, l_y) \quad (7)$$

and the prior is

$$p(t, x, y, \sigma_{\text{phot}}, ED, \mu, \sigma, \tau, l_x, l_y). \quad (8)$$

We form the posterior function by multiplying the likelihood and prior together:

$$p(ED, \mu, \sigma, \theta|F) \propto p(F|ED, \mu, \sigma, \theta)p(ED, \mu, \sigma, \theta) \quad (9)$$

where we have replaced the variables and parameters other than eclipse depth by θ for shorthand.

First, note that the likelihood function does not depend on the hierarchical parameters directly, so we can remove μ and σ from the brackets of the likelihood function. Second, the eclipse depth depends on the hierarchical parameters in this way:

$$p(ED|\mu, \sigma) = \frac{p(ED, \mu, \sigma)}{p(\mu, \sigma)}, \quad (10)$$

where we have made use of Bayes' theorem.

This means we can rewrite the likelihood and prior to obtain:

$$p(ED, \mu, \sigma, \theta|F) \propto p(F|ED, \theta)p(ED|\mu, \sigma)p(\mu, \sigma, \theta). \quad (11)$$

It is this refactoring that makes a hierarchical model different from a non-hierarchical one.

To form the posterior of the full hierarchical model, we multiply

the individual eclipse posteriors together:

$$\prod_{i=1}^n p(ED_i, \mu, \sigma, \theta_i | F_i) \propto p(\mu, \sigma) \prod_{i=1}^n p(F_i | ED_i, \theta_i) p(ED_i | \mu, \sigma) p(\theta_i) \quad (12)$$

where n is the number of eclipse observations— 10 in the case of the XO-3b dataset.

2.5 Hamiltonian Monte Carlo

We used the probabilistic programming package PyMC3 to build and sample from the model. PyMC3 uses Hamiltonian Monte Carlo (HMC), the state-of-the-art Markov Chain Monte Carlo (MCMC) algorithm, to perform the sampling. HMC is more efficient than other MCMC algorithms, meaning it can effectively describe the posterior using fewer samples than other MCMC algorithms. For high dimensional models, and especially for high dimensional hierarchical models, HMC is all but necessary (Betancourt & Girolami 2013).

Hamiltonian Monte Carlo works by exploiting the fact that for every probabilistic system we care about, there is an equivalent physical system that is easier to reason about (Betancourt 2017). The chains in an MCMC sampler move through parameter space to estimate the shape of the posterior; an equivalent physical system is the motion of a satellite orbiting a giant planet where the planet represents the mode of the probability distribution. The crucial step in HMC is to transform these trajectories from parameter space to momentum space using the Hamiltonian of the system, and sample from that instead. The HMC chains traverse through the typical set of the distribution, roughly defined as where most random draws from the model of interest would lie.

To use Hamiltonian Monte Carlo, the gradient of the likelihood function, with respect to the parameters, is needed in order to construct the Hamiltonian of the system. PyMC3 does this using Theano, which is a deep learning library that allows for efficient manipulation of matrices (The Theano Development Team et al. 2016). In our case the eclipse expressions reduce to the analytic expressions of Mandel & Agol (2002), but STARRY allows for analytic expressions and gradients in the general case of eclipse and phase mapping.

The biggest advantage is that HMC can diagnose problematic posteriors or models. Posteriors with pathological regions, such as high curvature, are hard for typical MCMC samplers to explore efficiently; hierarchical models exhibit such pathologies. This can lead to biases in the final results, which is hard to diagnose because typical samplers will quietly sample away unbeknownst to the user. When an HMC chain gets stuck in a region of high curvature or otherwise behaves badly, it will diverge to infinity and the sampler keeps track of where this occurred. Divergences can often be eliminated by changing the HMC step size or by reparameterizing the model.

2.6 Model comparison: Information Criteria

It is common among exoplanet scientists to use the Bayesian Information Criterion (BIC) or Aikake Information Criterion (AIC) to perform model comparison and selection (Schwarz 1978; Akaike 1974). Both criteria use the maximum likelihood and a complexity term to penalize overly complex models. These two information criteria describe slightly different things— the AIC measures the relative predictive loss of a set of models, and the BIC measures

how close each model is to the true model. In practice (at least in exoplanet science), they typically yield similar conclusions.

A shortcoming shared by BIC and AIC is that they are accurate only when using flat priors, which are not recommended for most models (Gelman et al. 2017). The AIC also assumes that the posterior distributions are multivariate Gaussians. The priors are never flat for hierarchical models, which means we cannot use the AIC or BIC for model comparison.

A more general model comparison tool is the Widely Applicable Information Criterion (WAIC; Watanabe (2010)). The WAIC is Bayesian, uses the full fit posterior, and critically, makes no assumptions about the shape of the posterior or priors. The WAIC is easily computed from the full fit posterior (McElreath, R. 2020):

$$\text{WAIC}(\text{data}, \Theta) = -2 \left(\text{lppd} - \sum_i \text{var}_\theta (\log p(F_i | ED_i, \theta_i)) \right) \quad (13)$$

where Θ is the posterior, F_i stands for the i^{th} eclipse observation, data refers to the entire suite of observations, and lppd stands for the log-pointwise predictive-density,

$$\text{lppd} = \sum_i \log \left(\frac{1}{S} \sum_{s=0}^S p(F_i | ED_i, \theta_{i,s}) \right), \quad (14)$$

where S is the number of samples and $\theta_{i,s}$ is the S^{th} set of parameters for the i^{th} observation. The log predictive pointwise density is an estimate of how well the model would fit new, unseen data. The second term in the WAIC expression is a penalty term that penalizes overly complex models.

Once MCMC sampling has finished, the WAIC can be computed in a few lines of code using the MCMC chains. It is also possible to compute the standard error of the WAIC, something that is not possible with the BIC or AIC. If the difference in WAIC between two models is significantly larger than the standard error of the difference, then the model with the smaller WAIC is favoured over the other. If the difference in WAIC is smaller than the standard error of the difference, then the models make equally good predictions and there is no evidence to favour one over the other.

Since all modern secondary eclipse, transit, and phase curve analyses use Markov Chain Monte Carlo to sample and store the posterior draws, the WAIC is a better choice than BIC or AIC for model comparison.

2.7 Pooling the GP parameters

We hypothesized that fitting a common set of Gaussian process amplitude and length scales across the suite of eclipses would yield more precise eclipse depths by sharing information about the detector sensitivity across the observations. Because we used Hamiltonian Monte Carlo, it was feasible to fully marginalize over the Gaussian process hyperparameters. However, we found that the fitted eclipse depths had nearly identical means and standard deviations between the shared and non-shared detector models of XO-3b. In practice we adopted the shared GP model for XO-3b because it has fewer parameters and is therefore easier to sample.

2.8 Results

We fit the ten 4.5 μm eclipses of XO-3b with three models: a model where each eclipse observation had its own, separate eclipse depth parameter, one where we used a single, pooled eclipse depth for all the observations, and a hierarchical model. To fit each model, we

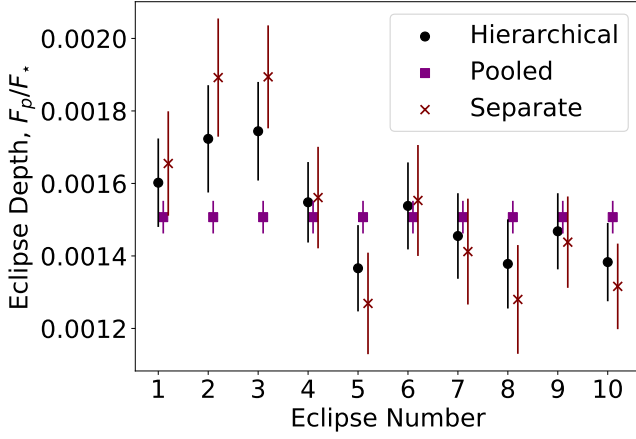


Figure 1. Eclipse depths of XO-3b for the three different models. The pooled model has the lowest eclipse depth uncertainty, but is not the best model according to the WAIC. The hierarchical model is the best model, and yields eclipses that are closer together, with lower uncertainties on the individual eclipse depths than the separate model (15% smaller on average). The hierarchical model represents a compromise between the overfit separate model and the underfit pooled model.

used 2000 tuning steps to initialize four HMC chains, and obtained 1000 samples for each chain. After sampling, we confirmed that the Gelman-Rubin statistic was close to 1 for all parameter values, and that there were no divergences. The eclipse depths from each model are shown graphically in Figure 1 and tabulated in Table 1. We also computed the WAIC values for each model, shown in Table 2.

The hierarchical model had a significantly lower WAIC than the separate model, and a marginally lower WAIC than the single eclipse depth (pooled) model. This suggests that the eclipse depths are indeed different between observations, but are more similar than if we had used a separate eclipse parameter to describe each. This also hints at some variability from observation to observation. Although the difference in WAIC between the hierarchical and fully pooled model is only $1.69 \sigma_{\Delta \text{WAIC}}$, typical hot Jupiters are predicted to show some epoch-to-epoch variability (Komacek & Showman 2020), which is another reason to adopt the hierarchical model over the pooled one.

The mean eclipse depth for the three models are consistent with one another within the uncertainties. In Figure 1, we see the effects of shrinkage on the eclipse depths. Compared to the separate model, the hierarchical model yields smaller scatter across the suite of eclipse depths and higher precision on the individual eclipse depths. Additionally, the individual uncertainties on the fitted eclipse depths are smaller by 15% on average in the hierarchical fits compared to the separate fits. The individual eclipse depth observations help constrain the others by shrinking the whole suite of eclipse depths towards the grand mean, but not as much as in the completely pooled model.

Table 1. Best-fit eclipse depths from each model of the ten *Spitzer* IRAC channel 2 eclipses of XO-3b. The parameters μ and σ are the hierarchical mean and standard deviation for the suite of eclipse depths. With the pooled model, we are implicitly assuming $\sigma = 0$, while for the separate model we are implicitly assuming $\sigma = \infty$. The hierarchical model fits for the amount of pooling, and is preferred over both the completely pooled and separate models.

Eclipse Number	Hierarchical	Pooled	Separate
1	1602±122	1507±45	1655±144
2	1723±148	1507±45	1892±163
3	1744±136	1507±45	1894±142
4	1548±111	1507±45	1561±140
5	1366±119	1507±45	1269±140
6	1538±120	1507±45	1553±153
7	1455±118	1507±45	1412±146
8	1378±123	1507±45	1280±150
9	1468±105	1507±45	1438±126
10	1383±108	1507±45	1316±118
μ	1520±81	1507±45	1527±219
σ	193±80	0	∞

Table 2. Comparison of different information criteria for the three XO-3b eclipse depth models— lower values are better. For the WAIC we also tabulate the standard error in the difference between each model. Using the BIC and AIC the pooled model is preferred. However, our model does not satisfy the assumptions necessitated by the BIC and AIC. The WAIC is more robust. According to the WAIC, the hierarchical model is the preferred model.

Model	Δ WAIC	$\sigma_{\Delta \text{WAIC}}$	Δ AIC	Δ BIC
Hierarchical	0.0	0.0	7.46	10.80
Pooled	8.54	5.04	0	0
Separate	65.66	25.60	20.31	23.03

3 HIERARCHICAL MODEL FOR MULTIPLE PLANETS

While hierarchical modelling is most obviously applicable for repeated measurements of the same planet, we can also extend it to secondary eclipse observations of multiple planets. We considered the published dayside brightness temperatures from Garhart et al. (2020), the largest dataset of uniformly analyzed hot Jupiter secondary eclipses.

We expect that hot Jupiter dayside temperatures, T_d , are approximately proportional to their irradiation temperatures, $T_0 = T_{\text{eff}} \sqrt{\frac{R_*}{a}}$. We built a hierarchical model by including this intuition in our hyperprior, and making the hierarchical mean a function of irradiation temperature:

$$\mu_d = m(T_0 - \langle T_0 \rangle) + b,$$

where $\langle T_0 \rangle$ is the average irradiation temperature. In other words, our hierarchical mean is now a line described by a slope and standard deviation. We represent the scatter about this line using the hyperparameter σ_d . The prior on each dayside brightness temperature is then $T_{d,p} \sim \mathcal{N}(\mu_d, \sigma_d)$.

For this hierarchical model, the hierarchical mean itself depends on two hyperparameters, the slope and intercept of the line, which we fit for simultaneously with the suite of dayside brightness temperatures. We used the following weakly informative priors for the hyperparameters: $m \sim \mathcal{N}(1, 0.5)$, $b \sim \mathcal{N}(2200K, 500K)$, $\sigma_d \sim \text{Half-}\mathcal{N}(500K)$.

We included the planets that had measurements at both 4.5 μm and 3.6 μm , which gave a total of 34 planets. The planets WASP-14b, WASP-19b, and WASP-103b had two sets of eclipses in both chan-

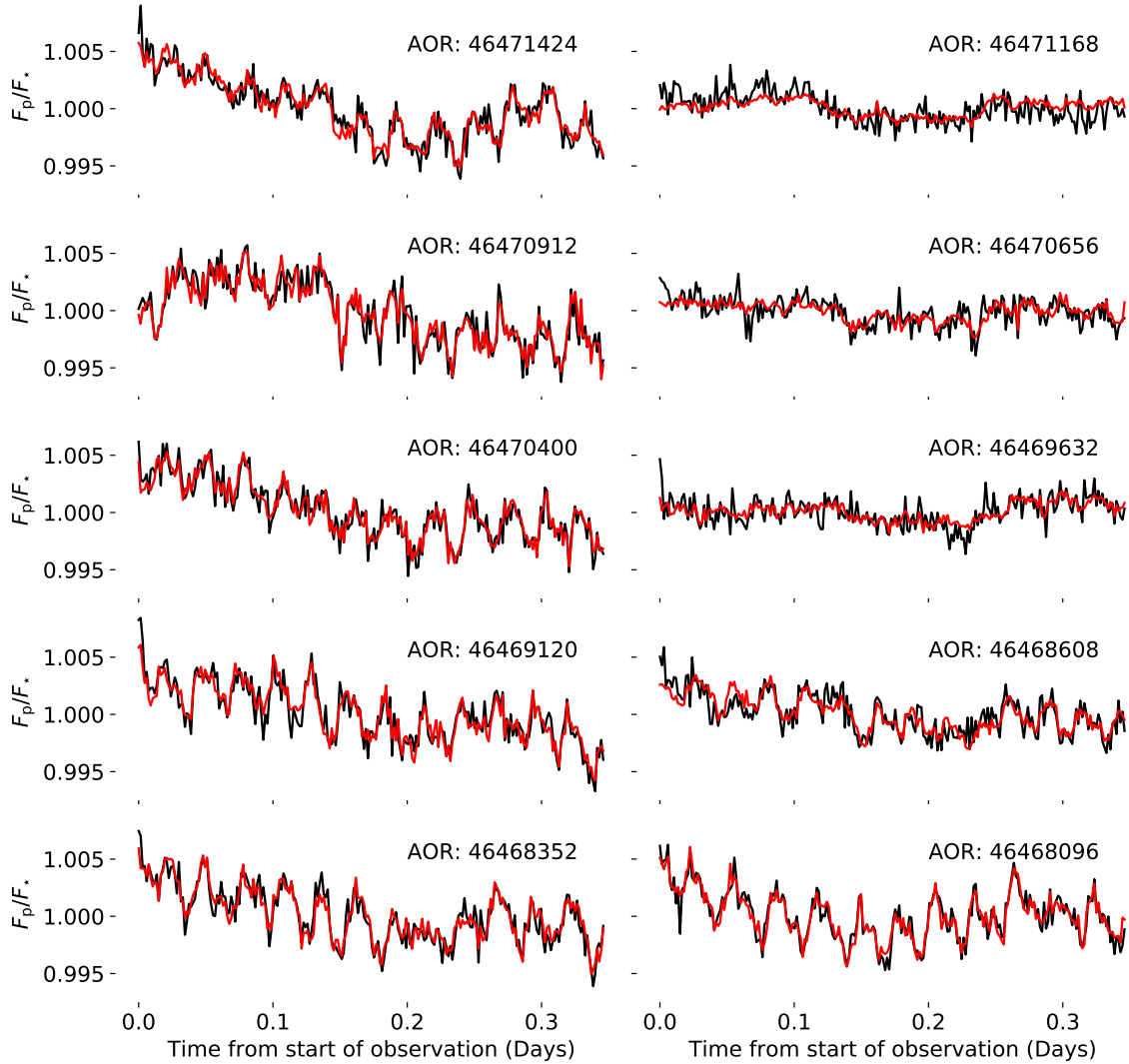


Figure 2. The full fit to each of the ten XO-3b eclipses, using the hierarchical model for the eclipse depths and a pooled Gaussian process for the detector systematics.

nels, so in total there were 74 measurements. Fitting 74 eclipse observations simultaneously with a two-dimensional Gaussian process is computationally intractable, so we took the published measurements at face value rather than refit them.

We again used PyMC3, and first fit a non-hierarchical model as our baseline, using separate $T_{d,p}$ parameters for each measurement. As expected, this model just reproduces the published dayside temperatures and uncertainties. This also acts as a confidence check that our priors are not biasing the fitted parameters.

Since there are measurements at two different wavelengths, we fit two different versions of the hierarchical model. In the wavelength dependent model, we allowed the dayside brightness temperature distributions to be different between the two wavelengths, fitting one set of hierarchical parameters for the $4.5 \mu\text{m}$ measurements, and another set for the $3.6 \mu\text{m}$ measurements. In the wavelength independent model, we used a common distribution for all the measurements, and thus one set of hierarchical parameters. We tabulate the refit brightness temperatures in Table 3. The WAIC values for the three models for the Garhart et al. (2020) dataset are tabulated in Table 4. The two hierarchical models are both significantly favoured over the non-

hierarchical model, but were not distinguishable from each other. The fitted values from the wavelength independent hierarchical model can be seen in Figure 4. The effects of Bayesian shrinkage are evident; the refit measurements are closer together, and more precise. We also plot the scaled dayside brightness temperatures in Fig 5.

The wavelength dependent model is indistinguishable from the wavelength independent model, according to the WAIC, meaning they make equally good predictions. In the wavelength independent model, the dayside brightness temperatures for both channels follow the same slope, or equivalently, the ratio of the slopes for each channel is equal to one. Our interpretation of this is that we are not detecting the trend of increasing brightness temperature ratio versus stellar irradiation reported by Garhart et al. (2020) and Baxter et al. (2020). The best-fit hierarchical parameters from our wavelength independent model are $\mu_d = 1.43 \pm 0.07$, $b = 2123 \pm 25\text{K}$, and $\sigma_m = 150 \pm 22\text{K}$. These constraints make it possible to empirically predict a planet’s brightness temperature in the *Spitzer* channels 1 or 2 bandpass given its irradiation temperature.

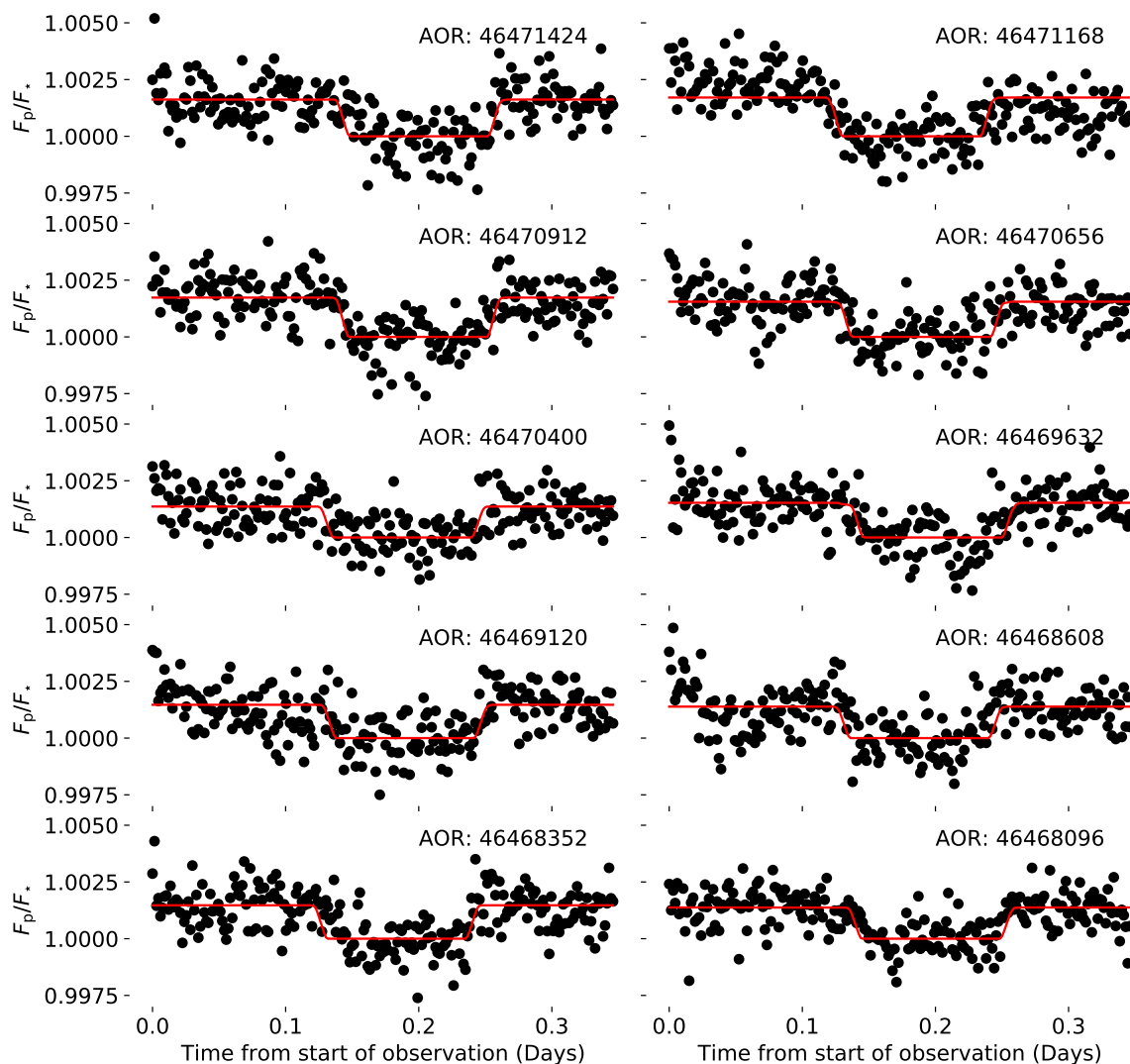


Figure 3. The ten XO-3b eclipses with the detector systematics removed using a Gaussian process as a function of stellar centroid location. The eclipse signal is clearly visible in the corrected raw data (represented by the black dots), and the best fit eclipse signal for each is shown as the red line.

4 DISCUSSION AND CONCLUSIONS

In our reanalysis of the ten secondary eclipses of XO-3b, we found that the hierarchical model was favoured. This means that the measured eclipse depths are indeed different from epoch to epoch, yet clustered. The biggest difference compared to previous analyses is that we were able to empirically fit for the amount of variability favoured by the data, and doing this improves the precision on our measurements by 15% on average, because of Bayesian shrinkage.

Hierarchical models could improve measurements of other hot Jupiters and other types of planets. They could be used to robustly test the reported variability in the secondary eclipses of the super earth 55 Cancri e (Demory et al. 2016; Tamburo et al. 2018), or to fit the twelve *Spitzer* eclipses of the recently discovered hot Saturn LTT 9779b (Dragomir et al. 2020). The published variability constraints for HD 189733b (Agol et al. 2010) and HD 209458b (Kilpatrick et al. 2020) could be revisited with hierarchical models, and the unpublished set of eleven *Spitzer* secondary eclipses of WASP-18b, which straddles the boundary between hot Jupiter and ultra hot Jupiter, could also benefit from a hierarchical treatment.

Repeated phase curve observations could be analyzed in a similar

way in order to search for variability. The hot Jupiter WASP-43b has one published (Stevenson et al. 2017; Mendonça et al. 2018; Morello et al. 2019; May & Stevenson 2020; Bell et al. 2020), and two unpublished, *Spitzer* phase curves at $4.5 \mu\text{m}$. A hierarchical model could be used to quantify the variability in the phase amplitudes and offsets of the three $4.5 \mu\text{m}$ phase curves.

We also showed that a hierarchical model is the best choice when fitting measurements from multiple planets in order to look for trends. For the Garhart et al. (2020) dataset, our two hierarchical models were significantly favoured over the non-hierarchical model. We did not detect the trend of increasing brightness temperature ratio with increasing stellar irradiation reported by Garhart et al. (2020); Baxter et al. (2020), but we did not rule it out. Additionally, we experimented with fitting the larger eclipse dataset from Baxter et al. (2020) with a hierarchical model, but the results were inconclusive: the hierarchical model did slightly better, but was indistinguishable from the non-hierarchical model according to the WAIC. Because the Baxter et al. (2020) sample is comprised of eclipses analyzed with disparate pipelines, we recommend that a wholesale reanalysis be performed to enable a more robust comparison.

Table 3. Results from fitting a wavelength independent hierarchical model to the [Garhart et al. \(2020\)](#) eclipse dataset.

Planet	T_0 (K)	$T_{d,ch2}$ (K)	$T_{d,ch1}$ (K)
HAT-13 b	2338±71	1802±119	1821±129
HAT-30 b	2430±48	1928±107	2008±99
HAT-33 b	2623±209	2073±119	2111±114
HAT-40 b	2505±54	1966±133	2007±140
HAT-41 b	2383±82	1725±97	1836±136
KELT-2 b	2434±51	1835±92	1971±88
KELT-3 b	2587±59	2108±99	2284±101
KELT-7 b	2908±44	2412±67	2492±64
Qatar-1 b	2011±51	1508±128	1488±143
WASP-12 b	3601±116	2995±92	3198±115
WASP-14 b	2677±85	2232±78	2267±74
WASP-14 b	2677±85	2276±78	2267±69
WASP-18 b	3417±82	3229±72	3034±58
WASP-19 b	2968±55	2342±115	2455±96
WASP-19 b	2968±55	2427±127	2464±90
WASP-36 b	2411±62	1854±145	1884±153
WASP-43 b	2042±57	1535±68	1740±62
WASP-46 b	2352±76	1883±134	1822±154
WASP-62 b	2025±47	1549±108	1694±122
WASP-63 b	2172±52	1613±137	1637±139
WASP-64 b	2367±239	1820±137	1958±126
WASP-65 b	2107±64	1561±150	1646±137
WASP-74 b	2718±65	2176±86	2097±79
WASP-76 b	3097±61	2725±56	2659±54
WASP-77 b	2372±40	1740±77	1806±73
WASP-78 b	3111±58	2621±143	2681±136
WASP-79 b	2489±72	1959±92	1968±98
WASP-87 b	3281±88	2878±108	2787±115
WASP-94A b	2133±106	1395±99	1454±80
WASP-97 b	2185±57	1635±86	1735±89
WASP-100 b	3121±240	2535±113	2490±119
WASP-101 b	2205±54	1606±104	1707±111
WASP-103 b	3554±69	3118±133	3022±111
WASP-103 b	3554±69	3057±127	2942±119
WASP-104 b	2123±267	1670±124	1650±122
WASP-121 b	3346±81	2611±62	2567±69
WASP-131 b	2069±45	1470±139	1530±146

Table 4. WAIC scores for the three models used to fit the suite of published eclipse depths from [Garhart et al. \(2020\)](#)— lower values are better. We also tabulate the standard error of the difference in WAIC between each model. The two hierarchical models both make equally good predictions, and significantly outperform the non-hierarchical model.

Model	Δ WAIC	$\sigma_{\Delta\text{WAIC}}$
Wavelength Dependent	0.0	0.0
Wavelength Independent	0.25	1.8
Separate	11.09	3.61

One obvious extension of our work, then, is to simultaneously refit the detector systematics and astrophysical signals for the entire suite of *Spitzer* secondary eclipses using an open source pipeline such as SPCA ([Bell et al. 2020](#)), and using a hierarchical model for the dayside brightness temperatures. This is computationally intractable using a two dimensional Gaussian process like we did for XO-3b, but it could potentially be done with an easier-to-compute detector model like Pixel Level Decorrelation ([Deming et al. 2015](#); [Garhart et al. 2020](#)), especially if Hamiltonian Monte Carlo is used.

In this work we have shown that hierarchical models are useful when analyzing repeated measurements from a single target, or when doing comparative exoplanetology studies of many targets. Next generation telescopes like *James Webb* and *Ariel* will make repeated

measurements of certain targets, and will both carry out photometric and spectroscopic transit, eclipse, and phase curve surveys for a variety of targets ([Bean et al. 2018](#); [Tinetti et al. 2018](#); [Charnay et al. 2021](#)). This will allow for atmospheric characterization of potentially thousands of more exoplanets, from Earth-like planets to ultra-hot Jupiters, and we recommend that these comparative surveys incorporate hierarchical modelling to make measurements and predictions that are as robust as possible.

ACKNOWLEDGEMENTS

D. K. and N. B. C. acknowledge support from McGill Space Institute and the Institut de recherche sur les exoplanètes. We have made use of open-source software provided by the Python, Astropy, SciPy, Matplotlib, and PyMC3 communities.

DATA AVAILABILITY

The reduced photometry for the ten archival secondary eclipse observations of XO-3b are freely available at <https://irachpp.spitzer.caltech.edu/page/data-challenge-2015>. The code used in the XO-3b reanalysis, and a Jupyter notebook showing

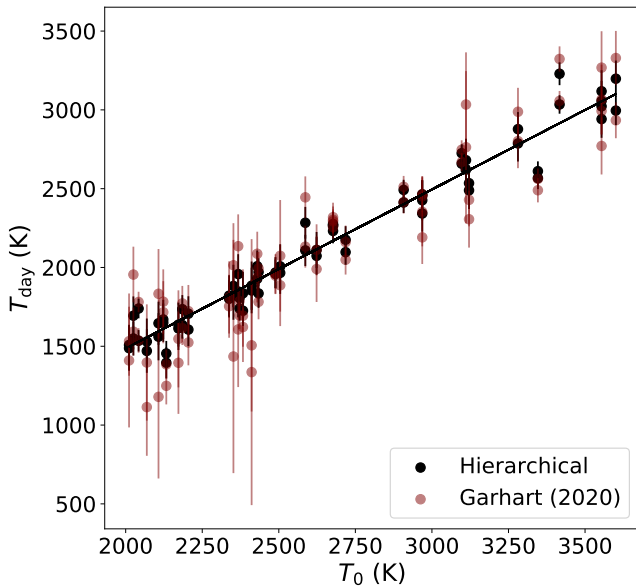


Figure 4. Dayside brightness temperatures for the planets analyzed by Garhart et al. (2020), refit with a wavelength independent hierarchical model. The red dots are the published values and the black line is the best fit trend line. The effects of Bayesian shrinkage are evident: the measurements are clustered closer to the line, and the uncertainties on the measurements are reduced.

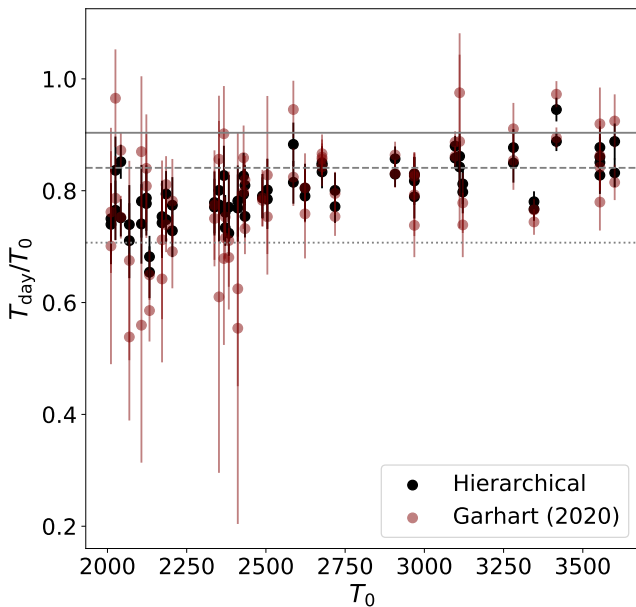


Figure 5. Dayside brightness temperatures from Fig 4, scaled by irradiation temperature. The horizontal lines represent some theoretical limits on dayside temperature assuming a zero Bond albedo: the solid line assumes zero heat recirculation, the dashed line assumes a uniform dayside hemisphere but a temperature of zero on the nightside, and the dotted line assumes a uniform temperature at every location on the planet.

the reanalysis of the Garhart et al. (2020) eclipses can both be found at <https://github.com/dylanskeating/HARMONiE>.

REFERENCES

- Agol E., Cowan N. B., Knutson H. A., Deming D., Steffen J. H., Henry G. W., Charbonneau D., 2010, *ApJ*, **721**, 1861
- Akaike H., 1974, *IEEE Transactions on Automatic Control*, **19**, 716
- Allard F., Homeier D., Freytag B., 2011, in Johns-Krull C., Browning M. K., West A. A., eds, *Astronomical Society of the Pacific Conference Series* Vol. 448, 16th Cambridge Workshop on Cool Stars, Stellar Systems, and the Sun. p. 91 ([arXiv:1011.5405](https://arxiv.org/abs/1011.5405))
- Baxter C., et al., 2020, *A&A*, **639**, A36
- Bean J. L., et al., 2018, *PASP*, **130**, 114402
- Bell T. J., et al., 2020, arXiv e-prints, p. [arXiv:2010.00687](https://arxiv.org/abs/2010.00687)
- Betancourt M., 2017, arXiv e-prints, p. [arXiv:1706.01520](https://arxiv.org/abs/1706.01520)
- Betancourt M. J., Girolami M., 2013, arXiv e-prints, p. [arXiv:1312.0906](https://arxiv.org/abs/1312.0906)
- Bonomo A. S., et al., 2017, *A&A*, **602**, A107
- Charnay B., et al., 2021, arXiv e-prints, p. [arXiv:2102.06523](https://arxiv.org/abs/2102.06523)
- Cowan N. B., Agol E., 2011, *ApJ*, **729**, 54
- Cowan N. B., Machalek P., Croll B., Shekhtman L. M., Burrows A., Deming D., Greene T., Hora J. L., 2012, *ApJ*, **747**, 82
- Deming D., et al., 2015, *ApJ*, **805**, 132
- Demory B.-O., Gillon M., Madhusudhan N., Queloz D., 2016, *MNRAS*, **455**, 2018
- Dragomir D., et al., 2020, *ApJ*, **903**, L6
- Evans T. M., Aigrain S., Gibson N., Barstow J. K., Amundsen D. S., Tremblin P., Mourier P., 2015, *MNRAS*, **451**, 680
- Fazio G. G., et al., 2004, *ApJS*, **154**, 10
- Garhart E., et al., 2020, *AJ*, **159**, 137
- Gelman A., Carlin J. B., Stern H. S., B. D. D., Vehtari A., Rubin D. B., 2014, *Bayesian Data Analysis*, (3rd ed.). Boca Raton : CRC Press
- Gelman A., Simpson D., Betancourt M., 2017, *Entropy*, **19**, 555
- Ingalls J. G., Krick J. E., Carey S. J., Laine S., Surace J. A., Glaccum W. J., Grillmair C. C., Lowrance P. J., 2012, in Clampin M. C., Fazio G. G., MacEwen H. A., Oschmann Jacobus M. J., eds, *Society of Photo-Optical Instrumentation Engineers (SPIE) Conference Series* Vol. 8442, *Space Telescopes and Instrumentation 2012: Optical, Infrared, and Millimeter Wave*. p. 84421Y, [doi:10.1117/12.926947](https://doi.org/10.1117/12.926947)
- Ingalls J. G., et al., 2016, *AJ*, **152**, 44
- Keating D., Cowan N. B., Dang L., 2019, *Nature Astronomy*, **3**, 1092
- Keating D., et al., 2020, *AJ*, **159**, 225
- Kilpatrick B. M., et al., 2020, *AJ*, **159**, 51
- Knutson H. A., et al., 2012, *ApJ*, **754**, 22
- Komacek T. D., Showman A. P., 2020, *ApJ*, **888**, 2
- Krick J. E., Fraine J., Ingalls J., Deger S., 2020, *AJ*, **160**, 99
- Lewis N. K., et al., 2013, *ApJ*, **766**, 95
- Luger R., Agol E., Foreman-Mackey D., Fleming D. P., Lustig-Yaeger J., Deitrick R., 2019, *AJ*, **157**, 64
- Mandel K., Agol E., 2002, *ApJ*, **580**, L171
- May E. M., Stevenson K. B., 2020, *AJ*, **160**, 140
- McElreath, R. 2020, *Statistical Rethinking*, (2nd ed.). Boca Raton : CRC Press
- Mendonça J. M., Malik M., Demory B.-O., Heng K., 2018, *AJ*, **155**, 150
- Morello G., Waldmann I. P., Tinetti G., Peres G., Micela G., Howarth I. D., 2014, *ApJ*, **786**, 22
- Morello G., Waldmann I. P., Tinetti G., 2016, *ApJ*, **820**, 86
- Morello G., Danielski C., Dickens D., Tremblin P., Lagage P. O., 2019, *AJ*, **157**, 205
- Morvan M., Nikolaou N., Tsiaras A., Waldmann I. P., 2020, *AJ*, **159**, 109
- Neil A. R., Rogers L. A., 2020, *ApJ*, **891**, 12
- Parmentier V., Crossfield I. J. M., 2018, *Exoplanet Phase Curves: Observations and Theory*. Springer International Publishing AG, [doi:10.1007/978-3-319-55333-7_116](https://doi.org/10.1007/978-3-319-55333-7_116)
- Sarkis P., Mordasini C., Henning T., Marleau G. D., Mollière P., 2021, *A&A*, **645**, A79
- Schwartz J. C., Cowan N. B., 2015, *MNRAS*, **449**, 4192

- Schwartz J. C., Kashner Z., Jovmir D., Cowan N. B., 2017, *ApJ*, **850**, 154
- Schwarz G., 1978, *Annals of Statistics*, **6**, 461
- Sing D. K., et al., 2016, *Nature*, **529**, 59
- Stevenson K. B., et al., 2012, *ApJ*, **754**, 136
- Stevenson K. B., et al., 2017, *AJ*, **153**, 68
- Tamburo P., Mandell A., Deming D., Garhart E., 2018, *AJ*, **155**, 221
- Teske J., et al., 2020, arXiv e-prints, p. [arXiv:2011.11560](https://arxiv.org/abs/2011.11560)
- The Theano Development Team et al., 2016, arXiv e-prints, p. [arXiv:1605.02688](https://arxiv.org/abs/1605.02688)
- Thorngren D. P., Fortney J. J., Lopez E. D., Berger T. A., Huber D., 2021, arXiv e-prints, p. [arXiv:2101.05285](https://arxiv.org/abs/2101.05285)
- Tinetti G., et al., 2018, *Experimental Astronomy*, **46**, 135
- Waldmann I. P., 2012, *ApJ*, **747**, 12
- Watanabe S., 2010, arXiv e-prints, p. [arXiv:1004.2316](https://arxiv.org/abs/1004.2316)
- Wong I., et al., 2014, *ApJ*, **794**, 134
- Zhang M., et al., 2018, *AJ*, **155**, 83

This paper has been typeset from a \TeX/L\AA\TeX file prepared by the author.